Range-dependent waveguide scattering model calibrated for bottom reverberation in a continental shelf environment

Ameya Galinde, Ninos Donabed, and Mark Andrews
Department of Electrical and Computer Engineering, Northeastern University, Boston, Massachusetts 02115

Sunwoong Lee and Nicholas C. Makris
Department of Mechanical Engineering, Massachusetts Institute of Technology, Cambridge, Massachusetts 02139

Purnima Ratilal
Department of Electrical and Computer Engineering, Northeastern University, Boston, Massachusetts 02115

An analytic model is developed for scattering from random inhomogeneities in range-dependent ocean waveguides using the Rayleigh–Born approximation to Green's theorem. The expected scattered intensity depends on statistical moments of fractional changes in compressibility and density, which scatter as monopoles and dipoles, respectively, and the coherence volume of the inhomogeneities. The model is calibrated for ocean bottom scattering using data acquired by instantaneous wide-area ocean acoustic waveguide remote sensing (OAWRS) and geophysical surveys of the ONR Geoclutter Program. The scattering strength of the seafloor on the New Jersey shelf, a typical continental shelf environment, is found to depend on wave number k, medium coherence volume V_c, and seabed depth penetration factor F_p following a $10 \log_{10}(F_p V_c k^4)$ dependence. A computationally efficient numerical approach is developed to rapidly compute bottom reverberation over wide areas using the parabolic equation by exploiting correlation between monopole and dipole scattering terms and introducing seafloor depth penetration factors. An approach is also developed for distinguishing moving clutter from statistically stationary background reverberation by tracking temporal and spatial fluctuations in OAWRS intensity images. © *2008 Acoustical Society of America.* [DOI: 10.1121/1.2832509]

I. INTRODUCTION

In this paper, we develop an analytic model with numerical implementation for reverberation in range-dependent ocean environments and bistatic source–receiver geometries. The model is derived from first principles using the acoustic wave equation for inhomogeneous media and by application of Green's theorem.

The model takes into account the full three-dimensional (3D) scattering interaction of the acoustic wavefield with volume or surface inhomogeneities. For efficiency, the model is implemented in terms of scattering from the spatially varying resolution footprint of the sonar, typically determined by beamforming and temporal matched filtering. Statistical moments of the randomly scattered field are expressed in terms of statistical moments of fractional changes in medium compressibility and density, and the waveguide Green function. Variations in compressibility and density lead to monopole and dipole terms, respectively. As the waveguide Green function is employed, the model directly incorporates attenuation in the sea bottom and scattering of evanescent waves by inhomogeneities.

The model is calibrated for ocean bottom reverberation with data acquired by instantaneous ocean acoustic waveguide remote sensing (OAWRS)[1,2] during the 2003 Main Acoustic Experiment and geophysical surveys of the ONR Geoclutter Program. The data were collected in the New Jersey Strataform,[3] south of Long Island, NY, a typical continental shelf environment with minimal bathymetric relief. The model is integrated to bathymetric databases to enable charting of predicted reverberation in geographic space. An approach is also developed for distinguishing moving clutter from statistically stationary background reverberation by tracking temporal and spatial fluctuations in OAWRS intensity images.

Analysis with the theory and data indicates that (a) both random fluctuations in seabed compressibility and density are important contributors to the scattered intensity and consequently reverberation, (b) the scattering strength of the seafloor on the New Jersey shelf, a typical continental shelf environment, is found to depend on wave number k, medium coherence volume V_c, and seabed depth penetration factor F_p following a $10 \log_{10}(F_p V_c k^4)$ dependence, where each term is a function of frequency.

A computationally efficient numerical approach is developed here to rapidly compute bottom reverberation over wide areas using the parabolic equation[4] by exploiting correlation between monopole and dipole scattering terms and introducing seafloor depth penetration factors. Without innovations of this kind, bottom reverberation models based on

volume scattering can be computationally intensive in range-dependent environments with bistatic source–receiver geometries because dipole scattering involves multidimensional spatial derivatives of the *complex* waveguide Green function. These typically must be computed numerically using large and dense 3D matrices.

A number of half-space models for seafloor scattering have used the Rayleigh–Born approach for local waterborne backscattering investigations.[5–8] Some monostatic range-independent models have used approximations similar to Rayleigh–Born.[8–11] Previous range-dependent waveguide reverberation models using the parabolic equation have only included monopole scattering with empirical models.[12–14]

II. ANALYTIC FORMULATION

Here we develop an analytic model for the scattered field from random medium inhomogeneities by application of Green's theorem. Assume the medium compressibility and density vary randomly in space, following a stationary random process within the local sonar resolution footprint.

Let the origin of the coordinate system be placed at the air–water interface with the positive z-axis pointing downward. Let the coordinates be defined by $\mathbf{r}_0 = (x_0, y_0, z_0)$ for the source, $\mathbf{r} = (x, y, z)$ for the receiver, and $\mathbf{r}_t = (x_t, y_t, z_t)$ for the centroid of an inhomogeneity. Spatial cylindrical (ρ, ϕ, z) and spherical systems (r, θ, ϕ) are defined by $x = r\sin\theta\cos\phi$, $y = r\sin\theta\sin\phi$, $z = r\cos\theta$ and $\rho^2 = x^2 + y^2$. The acoustic wave number k is given by the angular frequency $\omega = 2\pi f$ divided by the sound speed c.

A. Time harmonic scattered field moments

In the presence of volume inhomogeneities, the time-harmonic acoustic field $\Phi_t(\mathbf{r}_t, f)$ satisfies an inhomogeneous Helmholtz equation,[15]

$$\nabla^2 \Phi_t(\mathbf{r}_t, f) + k^2 \Phi_t(\mathbf{r}_t, f)$$
$$= -k^2 \Gamma_\kappa(\mathbf{r}_t) \Phi_t(\mathbf{r}_t, f) - \nabla \cdot [\Gamma_d(\mathbf{r}_t) \nabla \Phi_t(\mathbf{r}_t, f)], \quad (1)$$

where Γ_κ is the fractional change in compressibility,

$$\Gamma_\kappa(\mathbf{r}_t) = \frac{\kappa(\mathbf{r}_t) - \bar{\kappa}}{\bar{\kappa}}, \quad (2)$$

given compressibility $\kappa = 1/dc^2$, and Γ_d is fractional change in density,

$$\Gamma_d(\mathbf{r}_t) = \frac{d(\mathbf{r}_t) - \bar{d}}{d(\mathbf{r}_t)}, \quad (3)$$

where $\bar{\kappa}$ and $\bar{d}$ are the mean compressibility and density in the region, respectively.

Then, by application of Green's theorem, given a source at $\mathbf{r}_0$ and a receiver at $\mathbf{r}$, the time-harmonic scattered field $\Phi_s(\mathbf{r}_s | \mathbf{r}, \mathbf{r}_0, f)$ from inhomogeneities within the sonar resolution footprint V_s centered at $\mathbf{r}_s$ is[15]

$$\Phi_s(\mathbf{r}_s | \mathbf{r}, \mathbf{r}_0, f) = \int\int\int_{V_s} [k^2 \Gamma_\kappa(\mathbf{r}_t) \Phi_t(\mathbf{r}_t, f) G(\mathbf{r} | \mathbf{r}_t, f)$$
$$+ \Gamma_d(\mathbf{r}_t) \nabla \Phi_t(\mathbf{r}_t, f) \cdot \nabla G(\mathbf{r} | \mathbf{r}_t, f)] dV_t. \quad (4)$$

Here, $\Phi_t(\mathbf{r}_t, f)$ is the total field at the location of the inhomogeneity, and $G(\mathbf{r} | \mathbf{r}_t, f)$ is the medium's Green function. Elemental spatial variations in compressibility lead to monopole scattering, while those in density lead to dipole scattering. Density fluctuations contribute to both monopole and dipole scattering while sound speed fluctuations contribute only to monopole scattering.[15] The dipole term depends on spatial gradients of the total field and those of the Green function.

The total field at any location is a sum of the incident and the locally scattered fields,

$$\Phi_t(\mathbf{r}_t, f) = \Phi_i(\mathbf{r}_t | \mathbf{r}_0, f) + \Phi_s(\mathbf{r}_t, f), \quad (5)$$

where $\Phi_i(\mathbf{r}_t | \mathbf{r}_0, f) = (4\pi)^2 G(\mathbf{r}_t | \mathbf{r}_0, f)$. The $(4\pi)^2$ normalization factor yields the convenient source level of 0 dB re 1 μPa at 1 m. For small local perturbations in medium compressibility and density, the total field at the inhomogeneity can be approximated by the incident field in Eqs. (5) and (4). This is the first-order Rayleigh–Born approximation to Green's theorem. The randomly scattered field at the receiver can then be expressed as

$$\Phi_s(\mathbf{r}_s | \mathbf{r}, \mathbf{r}_0, f)$$
$$= 4\pi^2 \int\int\int_{V_s} [k^2 \Gamma_\kappa(\mathbf{r}_t) G(\mathbf{r}_t | \mathbf{r}_0, f) G(\mathbf{r} | \mathbf{r}_t, f)$$
$$+ \Gamma_d(\mathbf{r}_t) \nabla G(\mathbf{r}_t | \mathbf{r}_0) \cdot \nabla G(\mathbf{r} | \mathbf{r}_t, f)] dV_t, \quad (6)$$

which is a single-scatter approximation.

The mean scattered field from the inhomogeneities is

$$\langle \Phi_s(\mathbf{r}_s | \mathbf{r}, \mathbf{r}_0, f) \rangle$$
$$= (4\pi)^2 \int\int\int_{V_s} [k^2 \langle \Gamma_\kappa(\mathbf{r}_t) \rangle \langle G(\mathbf{r}_t | \mathbf{r}_0, f) G(\mathbf{r} | \mathbf{r}_t, f) \rangle$$
$$+ \langle \Gamma_d(\mathbf{r}_t) \rangle \langle \nabla G(\mathbf{r}_t | \mathbf{r}_0, f) \cdot \nabla G(\mathbf{r} | \mathbf{r}_t, f) \rangle] dV_t. \quad (7)$$

Random variables Γ_κ and Γ_d, are assumed to be independent of possible random fluctuations in the waveguide Green function.[16]

The second moment of the scattered field is

$$\langle |\Phi_s(\mathbf{r}_s | \mathbf{r}, \mathbf{r}_0, f)|^2 \rangle$$
$$= \langle \Phi_s(\mathbf{r}_s | \mathbf{r}, \mathbf{r}_0, f) \Phi_s^*(\mathbf{r}_s | \mathbf{r}, \mathbf{r}_0, f) \rangle$$
$$= \langle (4\pi)^4 \int\int\int_{V_s} [k^2 \Gamma_\kappa(\mathbf{r}_t) G(\mathbf{r}_t | \mathbf{r}_0, f) G(\mathbf{r} | \mathbf{r}_t, f)$$
$$+ \Gamma_d(\mathbf{r}_t) \nabla G(\mathbf{r}_t | \mathbf{r}_0, f) \cdot \nabla G(\mathbf{r} | \mathbf{r}_t, f)] dV_t$$
$$\times \int\int\int_{V_s'} [k^2 \Gamma_\kappa(\mathbf{r}_t') G^*(\mathbf{r}_t' | \mathbf{r}_0, t) G^*(\mathbf{r} | \mathbf{r}_t', f)$$
$$+ \Gamma_d(\mathbf{r}_t') \nabla G^*(\mathbf{r}_t' | \mathbf{r}_0, f) \cdot \nabla G^*(\mathbf{r} | \mathbf{r}_t', f)] dV_t' \rangle. \quad (8)$$

Equation (8) requires evaluation at two spatial locations $\mathbf{r}_t$

and $\mathbf{r}_t'$, which requires knowledge of the spatial correlation function of volume inhomogeneities. A variety of different forms have been assumed for this correlation function in the case of seabed inhomogenieties. They include Gaussian,[8] exponential,[17] as well as power law[7,8,10] correlation functions.

To capture the essential physics in a manner conducive to analysis, we assume that inhomogeneities are uncorrelated when the two points lie outside the coherence volume V_c and are fully correlated within this volume. This leads, for example, to

$$
\begin{aligned}
\langle \Gamma_k(\mathbf{r}_t)\Gamma_k(\mathbf{r}_t') \rangle \\
= V_c(\mathbf{r}_s,z_t)[\langle \Gamma_k^2(\mathbf{r}_t) \rangle - |\langle \Gamma_k(\mathbf{r}_t) \rangle|^2]\delta(\mathbf{r}_t - \mathbf{r}_t') \\
+ \langle \Gamma_k(\mathbf{r}_t) \rangle\langle \Gamma_k(\mathbf{r}_t') \rangle \\
= V_c(\mathbf{r}_s,z_t)\mathrm{Var}(\Gamma_k(\mathbf{r}_t))\,\delta(\mathbf{r}_t - \mathbf{r}_t') + \langle \Gamma_k(\mathbf{r}_t) \rangle\langle \Gamma_k(\mathbf{r}_t') \rangle.
\end{aligned}
\tag{9}
$$

Such delta function correlations are often used in theories of wave propagation in random media.[16,18] The coherence volume can be a function of horizontal position and depth. For example, overburden pressure in sediments leads to greater compaction with depth which affects coherence volume.[19]

Substituting equations similar to Eq. (9) into Eq. (8), leads to the second moment of the scattered field,

$$
\begin{aligned}
\langle |\Phi_s(\mathbf{r}_s|\mathbf{r},\mathbf{r}_0,f)|^2 \rangle \\
= |\langle \Phi_s(\mathbf{r}_s|\mathbf{r},\mathbf{r}_0,f) \rangle|^2 + \mathrm{Var}(\Phi_s(\mathbf{r}_s|\mathbf{r},\mathbf{r}_0,f)),
\end{aligned}
\tag{10}
$$

proportional to the total intensity, which is a sum of coherent and incoherent components. The relative importance of each of these terms within the sonar resolution footprint can be estimated by analysis similar to that in Appendix A of Ref. 16.

The coherent term is the square of the mean scattered field, the square of Eq. (7). The incoherent term is the variance of the scattered field,

$$
\begin{aligned}
&\mathrm{Var}(\Phi_s(\mathbf{r}_s|\mathbf{r},\mathbf{r}_0,f)) \\
&= (4\pi)^4 \int\int\int_{V_s} V_c(\mathbf{r}_s,z_t) \\
&\times [k^4\mathrm{Var}(\Gamma_k(\mathbf{r}_t))\langle |G(\mathbf{r}_t|\mathbf{r}_0,f)|^2|G(\mathbf{r}|\mathbf{r}_t,f)|^2 \rangle \\
&+ \mathrm{Var}(\Gamma_d(\mathbf{r}_t))\langle |\nabla G(\mathbf{r}_t|\mathbf{r}_0,f)\cdot\nabla G(\mathbf{r}|\mathbf{r}_t,f)|^2 \rangle \\
&+ k^2\mathrm{Cov}(\Gamma_k,\Gamma_d)\langle 2\Re\{G(\mathbf{r}_t|\mathbf{r}_0,f)G(\mathbf{r}|\mathbf{r}_t,f) \\
&\times \nabla G^*(\mathbf{r}_t|\mathbf{r}_0,f)\cdot\nabla G^*(\mathbf{r}|\mathbf{r}_t,f)\} \rangle]dV_t.
\end{aligned}
\tag{11}
$$

Measured reverberation from the sea bottom is often dominated by the incoherent term of Eq. (10). Exceptions occur, for example, when many scatterers with large impedence contrast, such as layers of gravel or rock on a sandy seafloor, fall within the sonar resolution footprint.

The approach presented may also be applied to model scattering from irregular interfaces between two media with differing sound speeds and densities. The volume integrals in

Eqs. (7) and (11) for this case would be replaced with surface integrals over the interface and the coherence volume V_c replaced by the coherence area A_c.[20]

B. Broadband scattered field moments

For a potentially broadband source function, analytic expressions are provided for the statistical moments of the scattered field from inhomogeneities within the sonar resolution footprint. Let $q(t)$ be the source wave form with Fourier transform $Q(f)$. The expected time-dependent scattered field $\Psi(\mathbf{r}_s|\mathbf{r},\mathbf{r}_0,t)$ is

$$
\langle \Psi_s(\mathbf{r}_s|\mathbf{r},\mathbf{r}_0,t) \rangle = \int_{-\infty}^{\infty} Q(f)\langle \Phi_s(\mathbf{r}_s|\mathbf{r},\mathbf{r}_0,f) \rangle e^{-j2\pi ft}df, \tag{12}
$$

by inverse Fourier transform of Eq. (7), weighted by the source spectrum.

From Parseval's theorem, the mean scattered energy over the resolution footprint is proportional to[21]

$$
\bar{E}(\mathbf{r}_s|\mathbf{r},\mathbf{r}_0) = \int |Q(f)|^2\langle |\Phi_s(\mathbf{r}_s|\mathbf{r},\mathbf{r}_0,f)|^2 \rangle df, \tag{13}
$$

where $\langle |\Phi_s(\mathbf{r}_s|\mathbf{r},\mathbf{r}_0,f)|^2 \rangle$ is obtained from Eq. (10).

Sea bottom reverberation is typically dominated by the incoherent intensity. In this case, only the variance term in Eq. (11) contributes to the total intensity in the right-hand side of Eq. (13).

III. APPLICATION TO SEAFLOOR REVERBERATION WITH CALIBRATION

In this section, we apply the scattering model developed in Sec. II to seafloor reverberation. Geophysical parameters of the model are calibrated with measured data.

A. OAWRS images of the ocean environment

Here we use OAWRS images obtained during the ONR-sponsored Main Acoustic Experiment 2003[1] on the U.S. East Coast continental shelf. A bistatic OAWRS system comprising of a vertical source array and a horizontally towed receiving array was deployed in the New Jersey Strataform located 200 km south of Long Island. The source array excited acoustic waveguides modes that propagated tens of kilometers in the continental shelf environment. Transmissions consisted of 1 s duration Tukey-shaded linear frequency modulated pulses in three different frequency bands; 390–440, 875–975, and 1250–1400 Hz. The transmissions were repeated every 50 s over the approximately 83 min duration it took to tow the receiving array along a 10 km track line at constant tow speed of 2 m/s. Data were collected over 5–6 tracks each day. Here we focus our analysis on data in the 390–440 Hz band as this was the wave form that was most frequently used for imaging.

Instantaneous OAWRS images of the ocean environment over wide areas spanning thousands of square kilometers are formed from each transmission. The arrivals are charted in range by two-way travel time and matched filter analysis, and in bearing by beamforming.[1,2] Scattered fields from objects at identical horizontal position but different

(a) OAWRS Data, Normalized Pressure Level
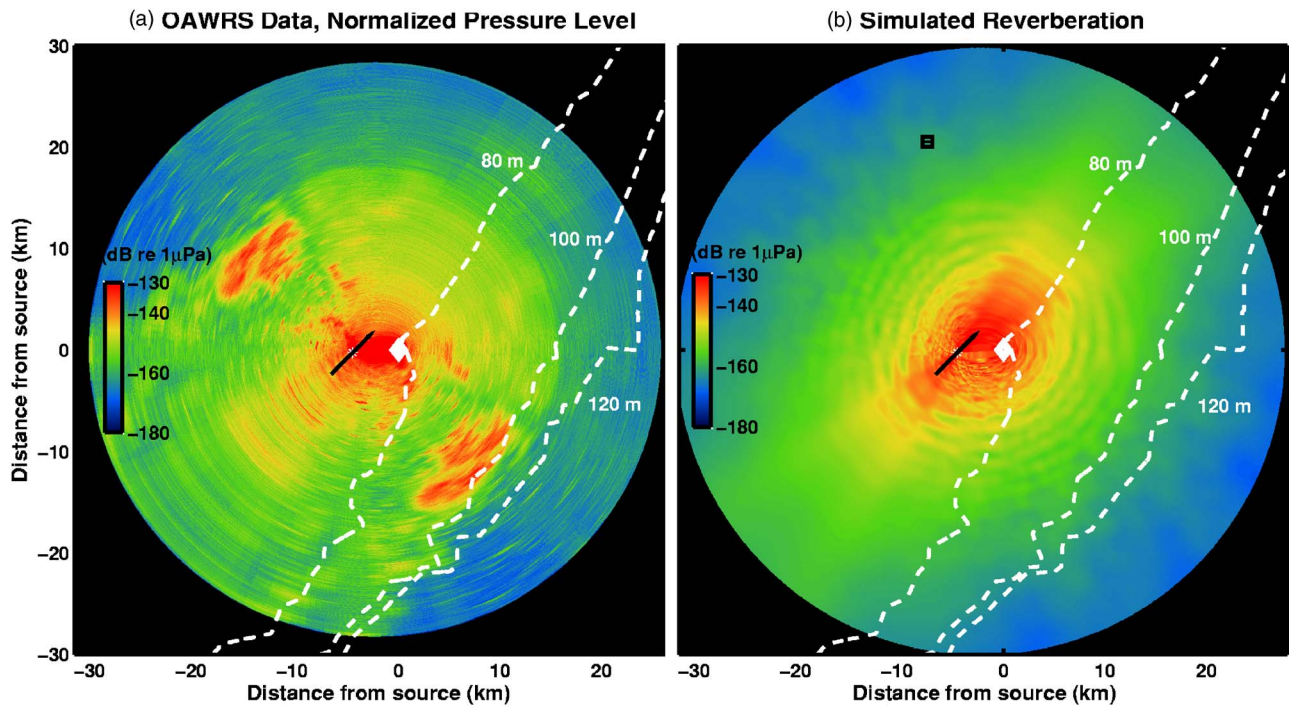
(b) Simulated Reverberation

FIG. 1. (Color online) (a) Instantaneous OAWRS image of the ocean environment on the New Jersey continental shelf. The image is averaged over five consecutive transmissions centered at 09:32 EDT, 14 May 2003. The imaging diameter of the system was set to roughly 60 km (40 s imaging time). The moored source (the white diamond) operating at 390–440 Hz is the coordinate origin at 39.0563N, 73.0365W. The towed horizontal receiving array moving along 51°E heading (indicated by black line) has 2.6° azimuthal resolution at array broadside and 15 m range resolution. The positive vertical axis points north. Depth contours are indicated by dashed lines. The image has been corrected for source level. (b) The simulated bottom reverberation corresponding to the data in (a), calculated using the computationally efficient approach at the center frequency 415 Hz with a typical observed sound speed profile. The small black 1 km by 1 km box shown near the upper left-hand corner indicates the location used for calibrating the reverberation model. This is the area shown in Fig. 6.

depths are integrated by the system in the resulting two-dimensional (2D) horizontal OAWRS images. The inherent left–right ambiguity in charting returns with a horizontal line array receiver is evident in some of the OAWRS images that will be presented here.

The resolution footprint of the OAWRS system is a function of both range and azimuth. The receiving array has a cross-range resolution given by $\rho\beta(\phi)$ where the angular resolution $\beta(\phi)$ is given by $\beta(\phi) \approx 1.44(\lambda/L\cos\phi)$ for broadside ($\phi=0$) through angles near endfire ($\phi=\pi/2$), where λ is the wavelength of the signal and L is the length of the array. At endfire, the angular resolution is given by $\beta(\phi=\pi/2) \approx 2.8\sqrt{\lambda/L}$. A Hanning spatial window was applied to the receiving array in the beamforming to reduce the levels of the sidelobes. The range resolution is $\Delta\rho=c/2B$ after matched filtering, where B is the signal bandwidth.[12]

The OAWRS images show scattered returns from large and densely populated fish groups, small or diffuse groups of fish, some discrete geologic features of the seafloor, as well as continuous diffuse returns from the seafloor. A typical image is shown in Fig. 1(a).[1] Trends in the images include the decay of scattered intensity with increasing bistatic range due to acoustic spreading loss and attenuation in the ocean waveguide, and spatial variation in cross-range resolution which leads to spatially varying blurring.

B. Estimating scattering level of the environment from OAWRS data

A challenge in analyzing sonar imagery is to distinguish diffuse background reverberation from discrete returns due to targets or clutter. The discrete returns may arise from surface or volume inhomogeneities such as marine creatures, geologic features, or man-made objects. It is often not known in advance from where in the water column the targets or clutter features arise.

To distinguish diffuse background reverberation from clutter and to compare the scattering level of returns from different ranges, we devise a two step approach. First, we detrend an OAWRS intensity image by correcting for mean transmission over the water-column, source level, and the spatially dependent resolution footprint of the OAWRS system. This leads to an estimate of what we call the environmental scattering level (ESL) at a given horizontal location. Next we compute statistics of ESL variations over space and time, and use these to discriminate diffuse background from clutter. We then investigate either the diffuse background or the clutter. Here we focus on the background.

Let $\overline{\mathrm{Lp}(\boldsymbol{\rho}_s|\mathbf{r},\mathbf{r}_0,t)}$ be $10\log_{10}$ of the OAWRS pressure squared matched filtered output centered at horizontal location $\boldsymbol{\rho}_s$ and time t, which may include some spatial and temporal averaging in pressure squared to reduce the variance. Then the $\mathrm{ESL}(\boldsymbol{\rho}_s,t)$ at the given location and time is obtained by

J. Acoust. Soc. Am., Vol. 123, No. 3, March 2008

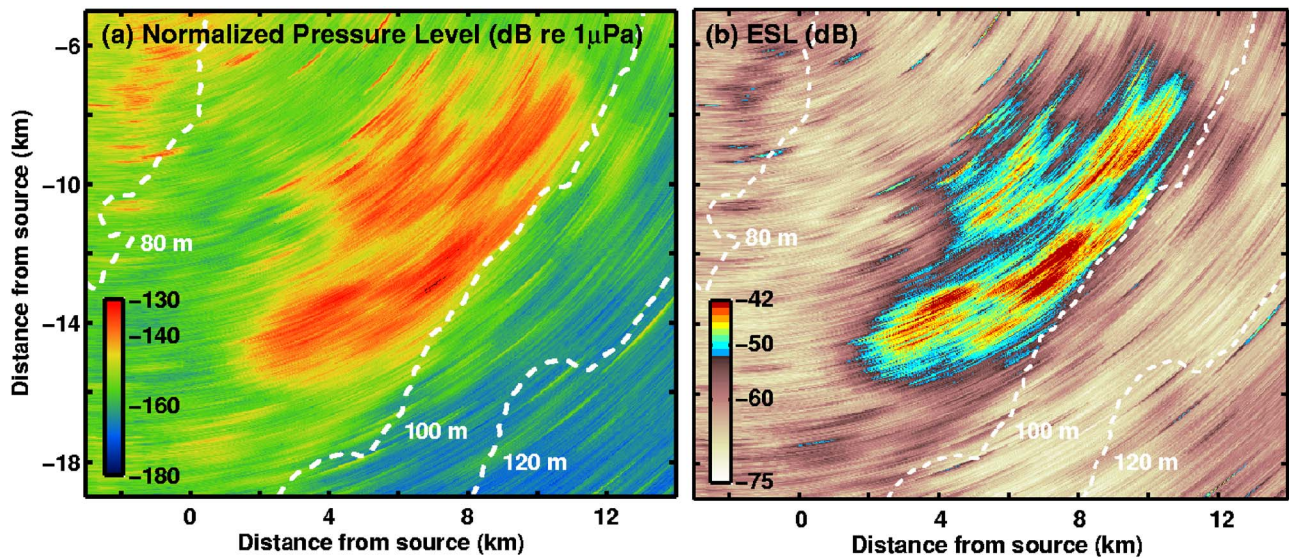Galinde *et al.*: Range-dependent waveguide reverberation model   1273

FIG. 2. (Color online) (a) A zoomed-in version of the OAWRS image shown in Fig. 1(a) in the south-east region containing a massive fish shoal. (b) Corresponding ESL image. Higher ESL levels are obtained in the region of dense fish shoal and lower levels correspond to the background. The transmission loss used for correcting this image is shown in Fig. 3(c).

$$\text{ESL}(\boldsymbol{\rho}_s, t) = \overline{\text{Lp}(\boldsymbol{\rho}_s | \mathbf{r}, \mathbf{r}_0, t)} - \text{SL}(\mathbf{r}_0) - \overline{\text{TL}(\boldsymbol{\rho}_s | \mathbf{r}_0)}$$
$$- \overline{\text{TL}(\mathbf{r} | \boldsymbol{\rho}_s)} - 10 \log_{10} A(\boldsymbol{\rho}_s), \qquad (14)$$

where $\overline{\text{TL}(\boldsymbol{\rho}_s | \mathbf{r}_0)}$ and $\overline{\text{TL}(\mathbf{r} | \boldsymbol{\rho}_s)}$ are $10 \log_{10}$ of the average of the antilog of transmission loss over the water column. The former is for transmission from source location to environmental location $\boldsymbol{\rho}_s$ and the latter is from this environmental location to the receiver. The spatially varying resolution footprint of the receiving array has area $A(\boldsymbol{\rho}_s) = [\beta(\phi)/2\pi][\pi(\rho + \Delta\rho)^2 - \pi\rho^2] \simeq \rho\beta(\phi)\Delta\rho$, and $\text{SL}(\mathbf{r}_0)$ is the source level. Environmental scattering level is then $10 \log_{10}$ of a ratio and has units simply of deciBels, like scattering strength.

Here we use a statistical propagation model based on the range-dependent parabolic equation[4] calibrated[22] against one-way transmission data from the same set of measurements to estimate the mean transmission loss over the water-column and obtain $\overline{\text{TL}(\boldsymbol{\rho}_s | \mathbf{r}_0)}$ and $\overline{\text{TL}(\mathbf{r} | \boldsymbol{\rho}_s)}$. Effects such as internal waves, eddies and turbulence cause fluctuations in ocean sound speed and density structure. These lead to scintillation in ocean acoustic waveguide propagation caused by changes in the multimodal interference structure. In this environment, the acoustic waveguide modes were found experimentally to become sufficiently randomized beyond roughly 2 km in range from the source[22] that the *expected* acoustic intensity varies only gradually with increasing range and does not exhibit the strong periodic modal interference structure in range and depth present in nonrandom waveguides.[16,20] The antilog of the mean transmission, $\overline{\text{TL}(\boldsymbol{\rho}_s | \mathbf{r}_0)}$ and $\overline{\text{TL}(\mathbf{r} | \boldsymbol{\rho}_s)}$ are proportional to the expected acoustic power transmitted through the waveguide at any given range and azimuth.

Figures 2(a) and 2(b) are OAWRS images of the mean matched filtered scattered intensity and the corresponding ESL of the ocean environment on 14 May 2003 after incoherently averaging intensity over five consecutive transmissions (pings) centered at time instance 9:32 Eastern Daylight Time (EDT). The ESL image in Fig. 2(b) is derived from Eq.

(14) where images corresponding to the right-hand side of Eq. (14) appear in Figs. 2(a) and 3. The mean transmission losses shown in Figs. 3(a) and 3(b) are in good agreement with measurements or models of transmission losses reported in Refs. 22–24 for the New Jersey Strataform.

In order to distinguish the statistically stationary background ESL from that due to moving biological clutter, we average N consecutive OAWRS images, which already were formed from five-ping running averages, to obtain a mean OAWRS image and a standard deviation OAWRS image over a wide spatial area. Figures 4(a) and 4(b) show the mean and standard deviation of $N = 361$ ESL images derived from data acquired within the frequency band from 390 to 440 Hz on 14 May 2003.[25]

We find in our 2003 OAWRS images that (a) high mean and high standard deviation characterizes regions where fish are regularly passing through, (b) high mean and low standard deviation characterizes regions where fish consistently remain, (c) low mean and high standard deviation characterizes regions where fish pass through intermittently, and (d) low mean and low standard deviation characterizes regions of diffuse reverberation from the seafloor. This can be seen in Fig. 5(a) where ESL is plotted as a function of sequential ping number for various spatial locations from Fig. 4(b). In particular, ESL in regions of dense fish population is roughly 20–25 dB higher than in regions where diffuse seafloor reverberation is the dominant scattering mechanism. Note that the above-mentioned (b) could also be caused by static geologic features but was ruled out in this experiment as data from the area shown in Fig. 4, six days prior, showed the scattered levels returning to those of the background when the massive fish shoal was absent.

For estimating the background ESL due to the seafloor, we focus analysis on regions with upslope bathymetry relative to the incident wave that had ambiguous regions that were downslope. This is to help eliminate the effect of left–right ambiguity, as seafloor scattering has been shown to be
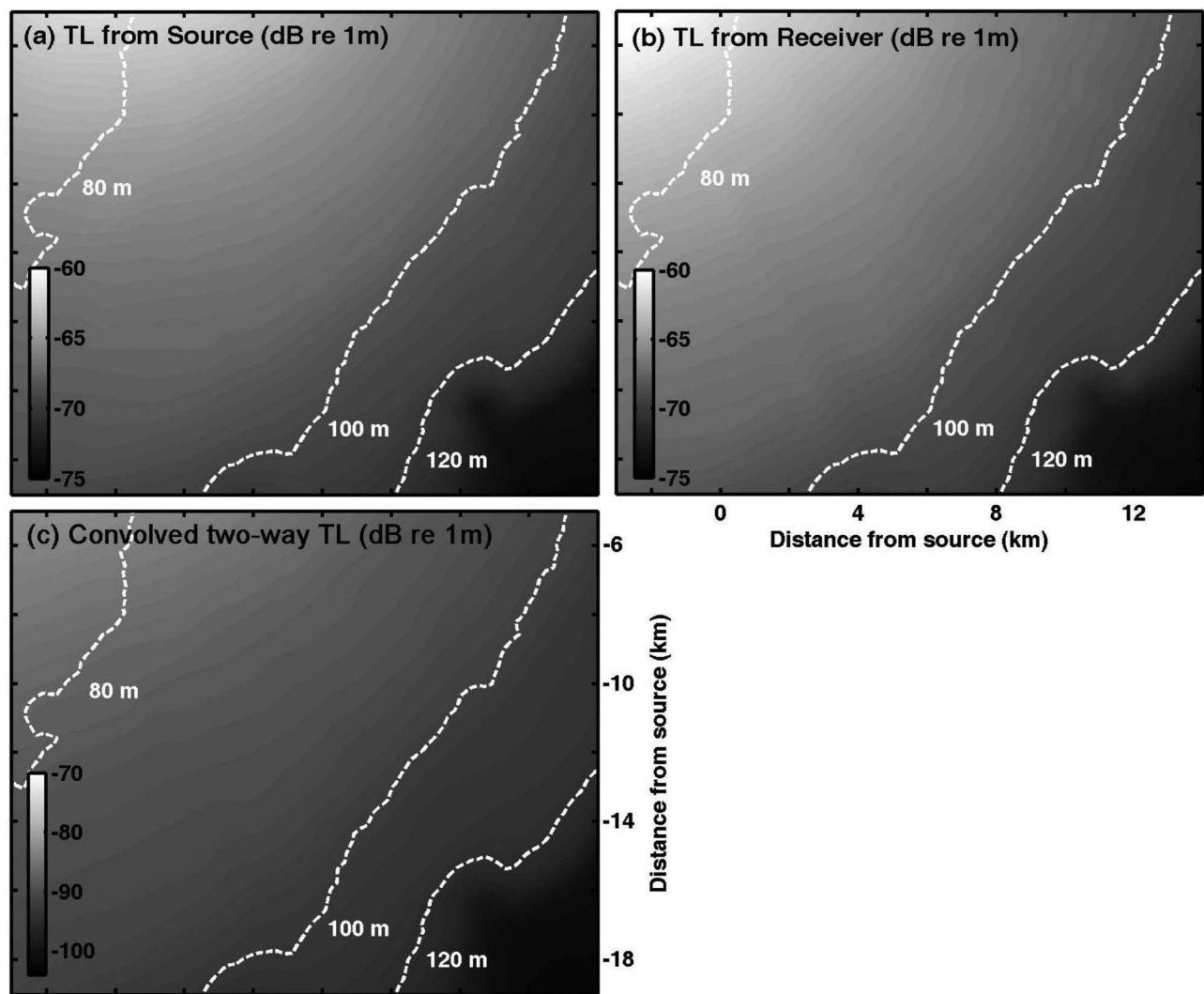
Galinde *et al.*: Range-dependent waveguide reverberation model

FIG. 3. (a) $\overline{\mathrm{TL}(\boldsymbol{\rho}_s|\mathbf{r}_0)}$ and (b) $\overline{\mathrm{TL}(\mathbf{r}|\boldsymbol{\rho}_s)}$ are 10 $\log_{10}$ of the mean antilog transmission losses over the water column from source and receiver respectively to the area shown for the 390–440 Hz band. (c) The quantities in (a) and (b) blurred with the spatially dependent resolution footprint of the receiving array.

more intense when bathymetry is upward sloping in the direction of the incident wave, and weaker when bathymetry is downward sloping,[13,14,26–29] as expected from physical principles. Temporal variations in ESL levels for various spatial locations with upslope bathymetry are shown in Fig. 5(b). The area shown in Fig. 4 consists of down sloping bathymetry but is shown to enable comparison of background ESL levels with those from fish shoal.

The mean seafloor ESL obtained here (and tabulated in the forthcoming Table II) can now be used to calibrate the reverberation model presented in Sec. II for seafloor scattering in the Strataform area. The standard deviation of ESL for seafloor scattering has been found by temporal and spatial averaging to be about 2 dB. This standard deviation will be useful in determining the accuracy of parameter estimates needed to calibrate the reverberation model.

C. Estimating geologic parameters necessary for reverberation model

The geological parameters necessary to implement the reverberation model defined in Eqs. (7) and (11) are estimated in the Appendix. In particular, the mean, standard de-

viation, and correlation of Γ_κ and Γ_d are estimated from the statistical moments of sound speed and density provided in Refs. 30, 31, and 3. The results, tabulated in Table I, are

TABLE I. Statistical geologic properties of the New Jersey Strataform used to calibrate the bottom reverberation model.

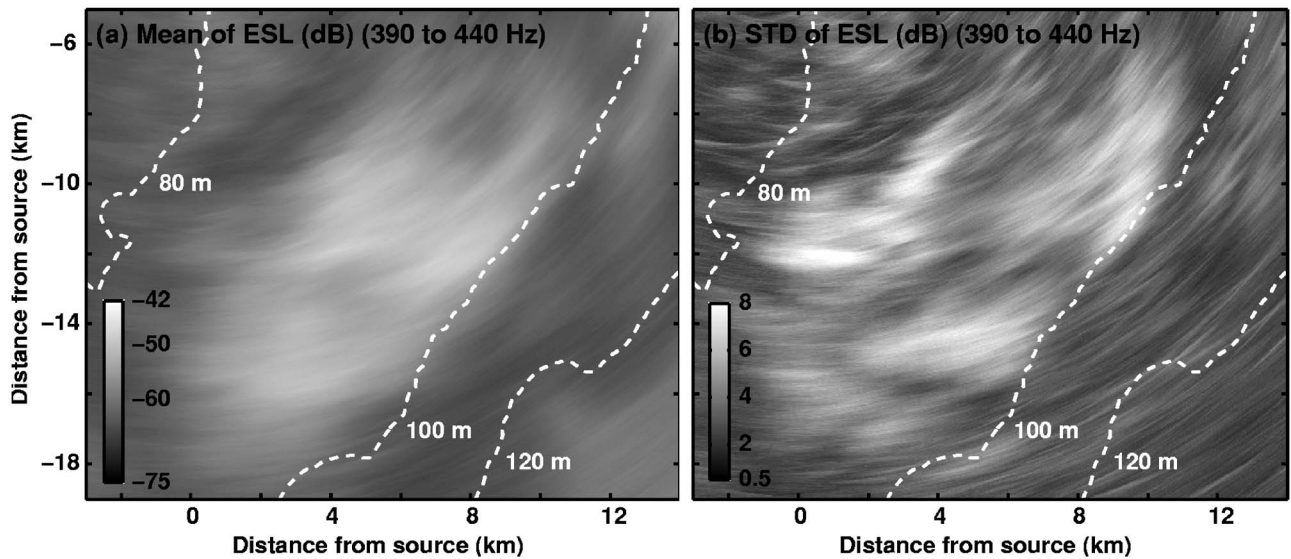| Statistical parameters	Average values over the region
$\bar{c}$ (m/s)	1700
σ_c (m/s)	35.5
$\mu^2 = \sigma_c^2/\bar{c}^2$	4.6889e−04
$\bar{d}$ (g/cm^3)	1.90
σ_d (g/cm^3)	0.16
$\eta^2 = \sigma_d^2/\bar{d}^2$	6.2e−3
$\langle \Gamma_\kappa \rangle$	0
$\langle \Gamma_\kappa^2 \rangle$	0.0083
Var(Γ_κ)	0.0083
$\langle \Gamma_d \rangle$	−0.0063
$\langle \Gamma_d^2 \rangle$	0.0066
Var(Γ_d)	0.0065
Cov(Γ_κ,Γ_d)	−0.0065

FIG. 4. Temporal and spatial variations in ESL for the area in Fig. 2 for data in the 390–440 Hz band collected on 14 May 2003. (a) Mean and (b) standard deviation of 361 ESL images formed from transmissions over a measurement time period ranging from 09:10 to 17:20 EDT.

consistent with those found in Ref. 7 which are based on measurements from ten different shallow and deep water sites around the world.

From Table I we observe that $\langle\Gamma_\kappa\rangle^2$ and $\langle\Gamma_d\rangle^2$ are at least 2 orders of magnitude smaller than $\mathrm{Var}(\Gamma_\kappa)$ and $\mathrm{Var}(\Gamma_d)$. The coherent term in Eq. (10) will therefore be negligible in comparison to the incoherent term. The total reverberation intensity can then be approximated as the variance of the scattered field using Eqs. (13) and (11).

D. Maximum likelihood estimator for coherence volume V_c

To implement the reveberation model in Eqs. (13) and (11) at a given location, an estimate is needed for the coherence volume V_c of the random seabed inhomogeneities. An

expression for the maximum likelihood estimator (MLE) for the coherence volume V_c in terms of the measured reverberation data and model is provided here.

The instantaneous scattered field measured at the receiver can be modeled as a circular complex Gaussian random variable.[32] The log transform of the matched filtered intensity within the resolution footprint centered at $\boldsymbol{\rho}_s$ then obeys a Gaussian probability density when the time-bandwidth product is sufficiently large,[32] as does the ESL,

$$p(\mathrm{ESL}(\boldsymbol{\rho}_s)|V_c)$$
$$= \left(\frac{\mu}{2\pi}\right)^{1/2}\exp\left(-\frac{\mu}{2}[\mathrm{ESL}(\boldsymbol{\rho}_s)-\langle\mathrm{ESL}(\boldsymbol{\rho}_s,V_c)\rangle]^2\right),$$

(15)

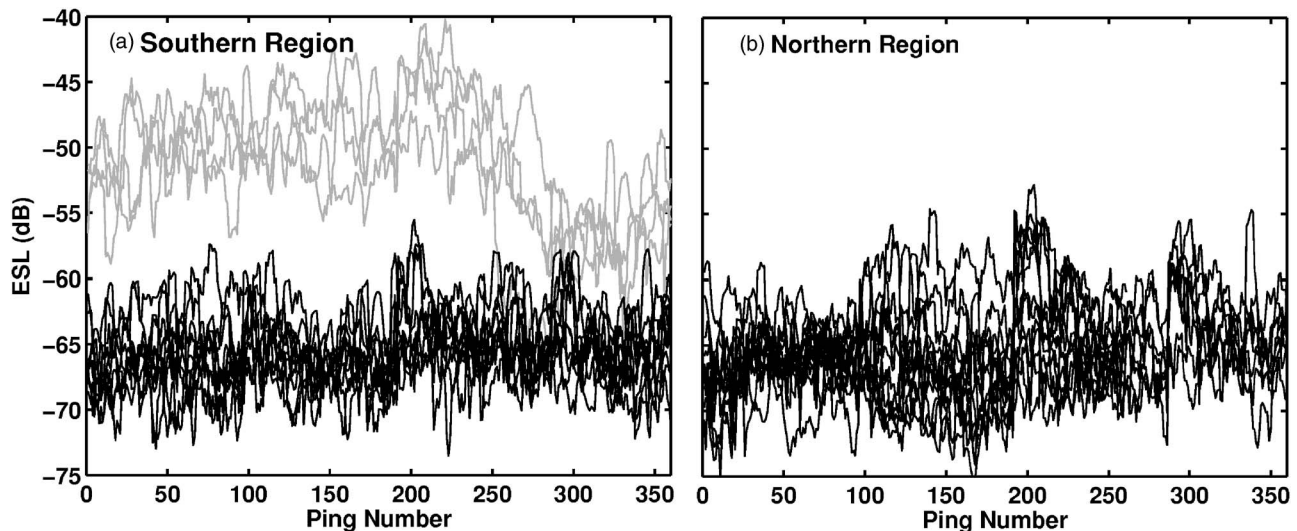where μ is the time–bandwidth product, which for the cur-

FIG. 5. (a) Temporal variation in ESL at various spatial locations as a function of transmission number or ping, for the image in Fig. 4. Gray lines in (a) are ESL at locations with persistently strong scattered returns from fish shoals. Black lines indicate ESL at locations consistent with the background. (b) Temporal variations in ESL for the region with upslope bathymetry in the vicinity of the small box shown in Fig. 1(b).

Galinde *et al.*: Range-dependent waveguide reverberation model

rent processing is greater than 10. This is because the matched filtered intensity data are averaged over two independent resolution cells and five independent pings.

As μ is large, the bias due to log transformation, defined in Eq. (22) of Ref. 32, is negligible. We can then make the approximation

$$\langle \text{ESL}(\boldsymbol{\rho}_s, V_c) \rangle = 10 \log_{10}(W(\boldsymbol{\rho}_s | \mathbf{r}, \mathbf{r}_0)) + 10 \log_{10}(V_c)$$
$$- \langle \text{TL}(\boldsymbol{\rho}_s | \mathbf{r}_0) \rangle - \langle \text{TL}(\mathbf{r} | \boldsymbol{\rho}_s) \rangle, \quad (16)$$

where we have introduced the new variable

$$10 \log_{10}(W(\boldsymbol{\rho}_s | \mathbf{r}, \mathbf{r}_0))$$
$$= 10 \log_{10}[\bar{E}(\boldsymbol{\rho}_s | \mathbf{r}, \mathbf{r}_0)] - 10 \log_{10}(V_c), \quad (17)$$

because it does not depend on V_c. Here, $\bar{E}(\boldsymbol{\rho}_s | \mathbf{r}, \mathbf{r}_0)$ is defined in Eq. (13), and is proportional to the total energy returned from the resolution footprint of range extent Δr. It is advantageous to express our intensity data in logarithmic units as it transforms signal-dependent noise into additive signal-independent noise.[32]

The ESL of the bottom measured in N different resolution footprints of OAWRS imagery for $s = 1, 2, 3, \ldots, N$ can be assumed to be independent and identically distributed. Their joint probability density function is

$$p(\text{ESL}(\boldsymbol{\rho}_1), \text{ESL}(\boldsymbol{\rho}_2), \ldots, \text{ESL}(\boldsymbol{\rho}_N) | V_c)$$
$$= \prod_{s=1}^{N} \left(\frac{\mu}{2\pi} \right)^{1/2} \exp\left(-\frac{\mu}{2} [\text{ESL}(\boldsymbol{\rho}_s) - \langle \text{ESL}(\boldsymbol{\rho}_s, V_c) \rangle]^2 \right). \quad (18)$$

The maximum likelihood estimator $\hat{V}_c$ for the coherence volume V_c is given by

$$\frac{d}{dV_c} \{ \ln[p(\text{ESL}(\boldsymbol{\rho}_1), \text{ESL}(\boldsymbol{\rho}_2), \ldots, \text{ESL}(\boldsymbol{\rho}_N) | V_c)] \} \Big|_{V_c = \hat{V}_c}$$
$$= 0. \quad (19)$$

Expanding Eq. (19) leads to

$$10 \log_{10}(\hat{V}_c)$$
$$= \frac{1}{N} \sum_{s=1}^{N} \text{ESL}(\boldsymbol{\rho}_s) - \frac{1}{N} \sum_{s=1}^{N} \{ 10 \log_{10}(W(\mathbf{r} | \mathbf{r}_0, \boldsymbol{\rho}_s))$$
$$- \text{TL}(\boldsymbol{\rho}_s | \mathbf{r}_0) - \text{TL}(\mathbf{r} | \boldsymbol{\rho}_s) \} \quad (20)$$

the desired estimator.

E. Reverberation model calibration

Implementation of the full reverberation model in Eq. (11) for range-dependent waveguides involves numerically calculating 3D spatial derivatives of the complex waveguide Green function. This leads to large 3D matrices that makes
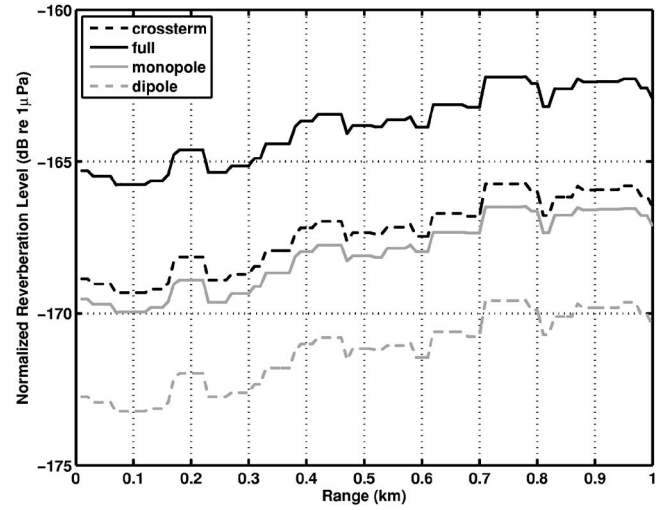

FIG. 6. Full bistatic, 390–440 Hz broadband, depth-integrated bottom reverberation model simulation for a horizontal transect across the 1 km by 1 km area shown in Fig. 1(b). The monopole term, dipole term, and crossterm contributions to the reverberation intensity are plotted for comparison.

the implementation cumbersome and reduces computational speed. For instance at 400 Hz, the spatial sampling required is approximately 0.2 m in range, 0.5 m in depth, and roughly 3° in azimuth for computational accuracy.

To avoid this problem, we calibrate the full reverberation model using only a small area, 1 km by 1 km, shown in Fig. 1(b). The coherence volume V_c is then determined with the approach outlined in Sec. III D. We provide a method for implementing the reverberation model that is computationally efficient over wide areas in the next section.

The scattered intensity of Eq. (11) is a sum of (1) a purely monopole term dependent on the variance of fractional change in compressibility, (2) a purely dipole term dependent on the variance of fractional change in density, and (3) the covariance between the two. The contribution of these three terms for a horizontal transect through the small area is shown in Fig. 6.

The MLE of the coherence volume $\hat{V}_c$ is summarized in Table II. We assume the inhomogeneites are isotropic, so that $V_c = \frac{4}{3} \pi l_c^3$, where l_c is the coherence radius. The coherence lengths in x, y, and z directions are $l_x = l_y = l_z = 2l_c$. The acoustically determined correlation length obtained here is comparable to the geologic correlation depth of between 0.3 and 3 m from analysis of core data.[33]

As the background ESL has a standard deviation of ± 2 dB, the estimate $10 \log_{10} \hat{V}_c$ also has the same standard deviation. This leads to a correlation length in the range from 15 to 21 cm. There could also be uncertainties in our estimates of the moments of Γ_κ and Γ_d. The variations in $\text{Var}(\Gamma_\kappa)$ needed to match the data over the range of uncertainty in the correlation length occupies roughly a factor of 2.

TABLE II. Estimates for the New Jersey Strataform. The standard deviation for ESL and SS is ± 2 dB.

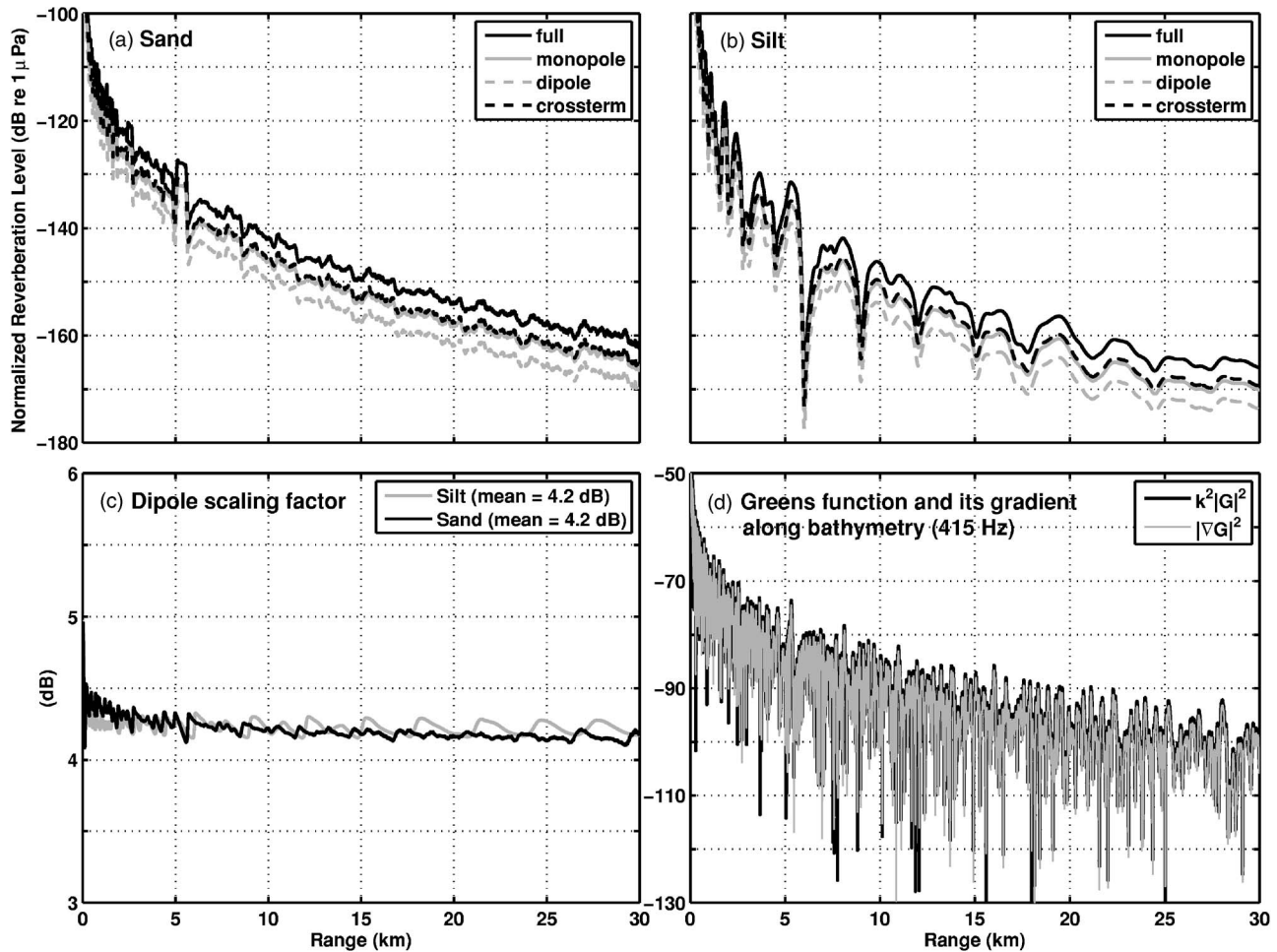| f (Hz)	ESL (dB)	V_c (m^3)	$2l_c$ (m)	f_d (dB)	f_p (m)	SS (dB)
390–440	−67.5	0.0030	0.18	4.2	0.46	−37

FIG. 7. Broadband 390–440 Hz, monostatic reverberation in Pekeris waveguides with (a) sand and (b) silt bottom for a 0 dB re 1 μPa at 1 m source level comprising of a single element at 50 m depth. The receiving array parameters are the same as those used in the experiment in Fig. 1(a). The Green function for Pekeris waveguides calculated using the normal mode code, Kraken (Ref. 36). (c) The dipole scaling factor equal to the ratio between the full term and the monopole term plotted in deciBels remain fairly constant to within ± 0.1 dB and is independent of the bottom type. (d) Comparison of the magnitudes of the Greens function and its spatial derivative at the water–sediment interface at 415 Hz.

Here we ignored a potential degradation due to matched filtering the data in an ocean waveguide while calibrating them with the reverberation model. This degradation is typically small, less than 3 dB for the ranges of interest.[22,34]

IV. COMPUTATIONALLY EFFICIENT IMPLEMENTATION

When working on a field experiment, it is often instructive to rapidly predict seabed reverberation over wide areas, to aid in experimental design. A computationally efficient approach for computing seabed reverberation in range dependent waveguides over wide areas is developed here. It is based on the introduction of a dipole scaling factor and a depth-penetration factor that simplify the numerical implementation.

We find it a good approximation to take the dipole and cross terms in the reverberant intensity of Eq. (11) to be proportional to the monopole term. This is illustrated for horizontally stratified Pekeris sand and silt waveguides in Figs. 7(a) and 7(b) with collocated source and receiver, and for the bistatic scenario in a range dependent waveguide in Fig. 6. The total intensity can be estimated from the mono-

pole term alone by multiplication with a constant factor, F_d, which we call the dipole scaling factor. This can be seen by noting in Fig. 7(c) that the ratio of the total intensity to the monopole term is a constant, with $10 \log_{10} F_d \approx 4.2$ dB. This approximation is a consequence of the fact that $|\nabla G|$ is proportional to $k|G|$, as shown in Fig. 7(c), which means that the dipole and monopole terms are proportional. Without this approximation, it is currently impractical to compute reverberation over wide areas because of the tremendous computational effort needed to determine the derivatives of the Green function in the dipole term.

The depth integral of Eq. (11) for volume scattering can be approximated by the seafloor surface contribution multiplied by a depth penetration factor, F_p. The depth penetration factor provides the equivalent depth over which acoustic intensity in the seabed is of similar magnitude as that on the seafloor, before it decays rapidly with depth due to sediment attenuation. This factor is simply the ratio of the volume integral to the seafloor contribution, which are shown in Figs. 8(a) and 8(b), with corresponding F_p ratio in Fig. 8(c), which is found to be dependent on bottom type, roughly
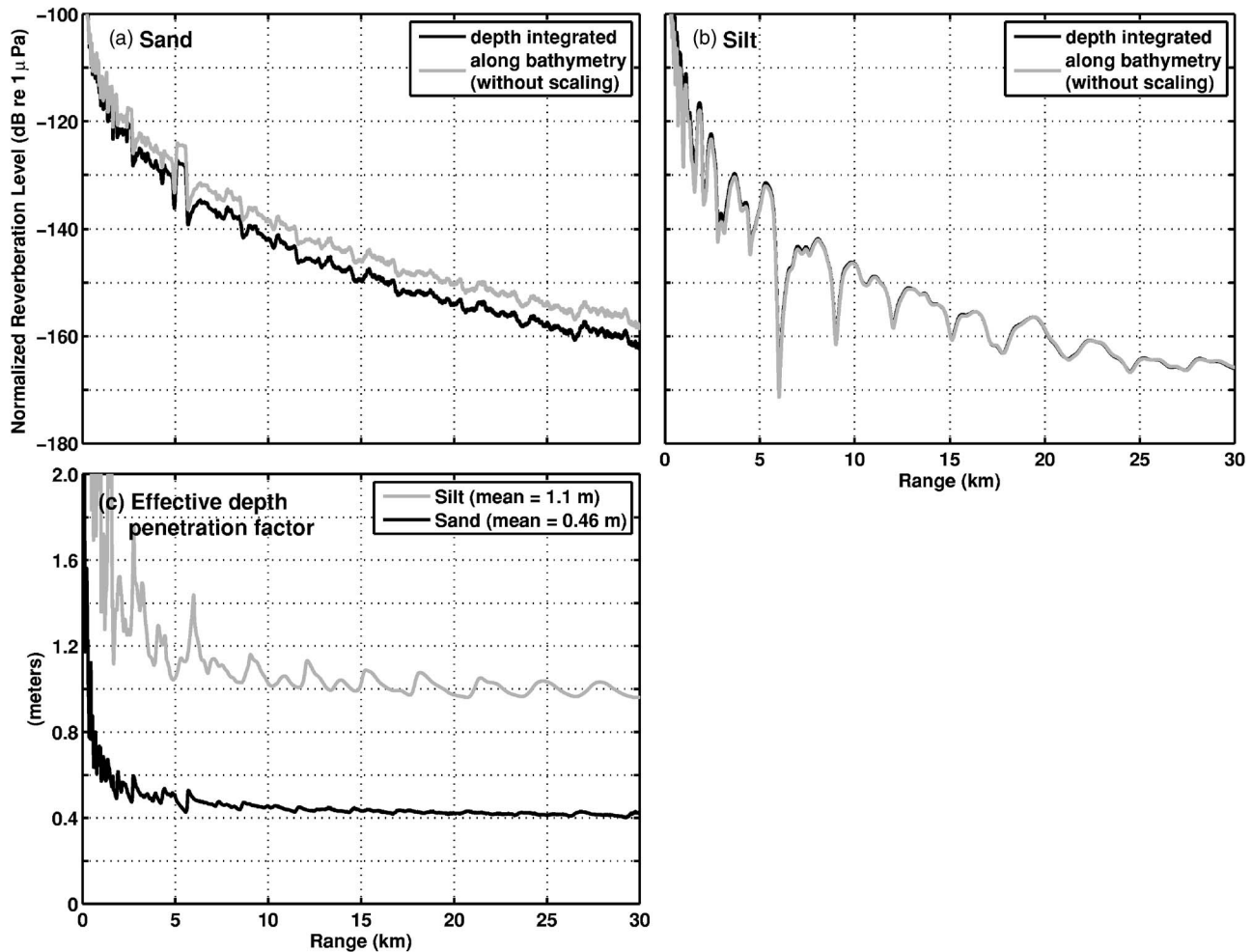
FIG. 8. Comparison of the 390–440 Hz broadband depth-integrated bottom reverberation intensity with the broadband intensity at the water–sediment interface in the Pekeris (a) sand and (b) silt waveguides. (c) The effective penetration depth in meters plotted for Pekeris sand and silt waveguides.

0.5 m for sand and 1 m for silt. The depth penetration factor is also a function of frequency, decreasing with increasing frequency.

Another approximation that can greatly increase computational efficiency is to calculate the scattered field at just the center frequency of the broadband signal. Figure 9 compares the full broadband depth integrated monostatic reveberation to the range-averaged scattered field at the center frequency with the two approximations introduced earlier applied to the result. The latter single frequency range-averaged approximation provides a good estimate to the broadband result.

The approximations made in this section require only the Green function magnitude on the seabed surface which can be stored in sparse 2D matrices rather than dense 3D matrices required for the full calculation. The reverberation intensity is accurate to within ±0.5 dB for ranges greater than 3 km and to within 3 dB for ranges between 1 and 3 km. Figure 1(b) illustrates this approach applied to model reverberation over wide areas on the New Jersey continental shelf corresponding to the OAWRS data Fig. 1(a). The reverberation levels from the simulation are comparable to the background levels in the data, especially in areas adjacent to the massive fish shoal.

V. SCATTERING STRENGTH

Here we derive the scattering strength (SS) of the bottom on the New Jersey continental shelf using the model and calibration results. As the seabed inhomogeneities have coherence lengths that are smaller than the wavelength,[35] we can apply the sonar equation to approximate SS of the bottom from Eq. (11) with the approximations introduced in Sec. IV as

$$\text{SS} \approx 10 \log_{10}[F_d F_p V_c k^4 \text{Var}(\Gamma_k)]. \tag{21}$$

The SS of the sandy bottom on the New Jersey Strataform is tabulated in Table II. Analysis with a normal mode propagation model[36] indicates that the first 10 modes are important contributors to the acoustic field at a range of 20 km from the source where the calibration was done. At this range, the depth-averaged intensity of mode 10 is about $1/5$ the depth-averaged intensity of mode 1. The grazing angles for modes 1–10 range from $2°$ to $12°$ and the derived SS level of roughly -37 ± 2 dB are determined by these grazing angles after long range propagation in the waveguide with the effect of multimodal coupling in the scattering process.
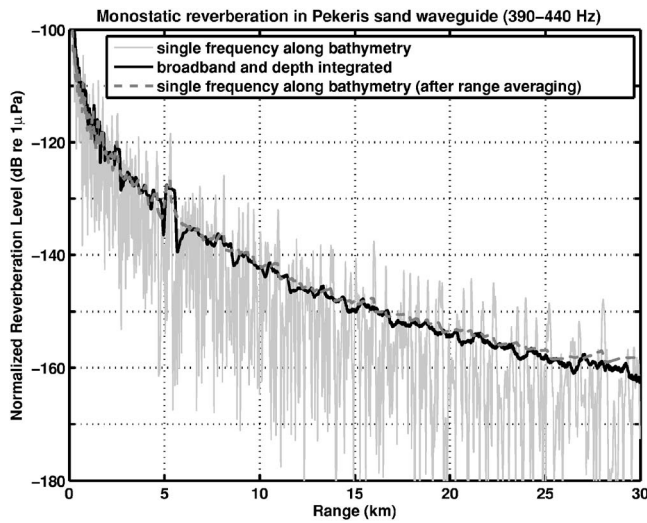
FIG. 9. Full 390–440 Hz broadband depth-integrated monostatic bottom reverberation compared to simulated result at center frequency 415 Hz calculated using efficient approach with the dipole scaling and depth penetration factors.

For reverberation measured at 390–440 Hz bandwidth considered in this paper, volume scattering is expected to be the dominant mechanism at all grazing angles for a sandy seabed as shown in Figs. 10 and 11 of Ref. 5. Our estimate agrees well with those of other ocean environments with sandy bottoms in Refs. 5 and 10, suggesting low surface roughness at this site and the consequent importance of evanescent energy in generating low-angle volume backscatter via subcritical ensonification.

The overall frequency dependence of SS in Eq. (21) is determined by the wave number k, which is directly proportional to frequency, the depth penetration factor f_p that decreases with increasing frequency, and potentially the coherence volume sampled by the acoustic wave V_c. The coherence volume may depend on frequency as short wavelength acoustic fields are more sensitive to small scale fluctuations in medium properties than long wavelength acoustic waves. This acoustically determined coherence volume may differ from the geologic coherence volume that is determined purely from spatial variations in medium properties.

VI. CONCLUSION

An analytic model for 3D, bistatic scattering from medium inhomogeneities is developed from first principles by application of Green's theorem. Statistical moments of the scattered field are expressed in terms of statistical moments of medium compressibility and density fluctuations. The model is applied to seabed reverberation and optimally calibrated with both OAWRS and geological data on the New Jersey continental shelf. Analysis with the model indicates that (1) seabed reverberation is incoherent, and (2) scattering strength varies with frequency depending on wavenumber k, medium coherence volume V_c and seabed depth penetration factor F_p following a $10 \log_{10}(F_p V_c k^4)$ dependence.

An efficient numerical approach is also developed for rapidly computing seabed reverberation over wide areas for bistatic sonar systems in range-dependent ocean waveguides.

It exploits the correlation between monopole and dipole scattering terms and the limited penetration of acoustic fields in the seabed. The model handles the scattering of evanescent waves in the seabed. Finally, an approach for distinguishing the statistically stationary background reverberation from the scattered fields of moving targets in sonar data by tracking the temporal and spatial evolution of the returns is presented.

APPENDIX: DERIVATION OF STATISTICS OF GEOACOUSTIC PARAMETERS

The seabed on the New Jersey Strataform is predominantly comprised of sand. It has been mapped by geophysical surveys with analysis provided in Refs. 3, 30, and 31. From these, we gathered the statistical moments of seabed sound speed and density fluctuations and list them in Table I. We assume that sound speed $c_t(\boldsymbol{\rho}_t) \sim N(\bar{c}, \sigma_c)$ and density $d_t(\boldsymbol{\rho}_t) \sim N(\bar{d}, \sigma_d)$ obey Gaussian random processes that are locally stationary in a given area. These statistical moments can vary between areas to account for potential changes in sediment type. We assume that sound speed and density are uncorrelated, which is a valid assumption given the large scatter in the data in Fig. 10(b) of Ref. 30. Despite this assumption, Γ_κ and Γ_d can still be correlated.

From Eqs. (2) and (3), the means are given by

$$\langle \Gamma_\kappa(\mathbf{r}_t) \rangle = 0 \tag{A1}$$

and

$$\langle \Gamma_d(\mathbf{r}_t) \rangle = 1 - \bar{d} \left\langle \frac{1}{d_t(\mathbf{r}_t)} \right\rangle, \tag{A2}$$

where $\bar{d}$ and $\bar{c}$ as defined before are the mean density and sound speed within the sonar resolution footprint, respectively. The second moments are given by

$$\langle \Gamma_d^2(\mathbf{r}_t) \rangle = 1 - 2\bar{d} \left\langle \frac{1}{d_t(\mathbf{r}_t)} \right\rangle + \bar{d^2} \left\langle \frac{1}{d_t^2(\mathbf{r}_t)} \right\rangle \tag{A3}$$

and

$$\langle \Gamma_\kappa^2(\mathbf{r}_t) \rangle = \frac{\left\langle \dfrac{1}{d_t^2(\mathbf{r}_t)} \right\rangle \left\langle \dfrac{1}{c_t^4(\mathbf{r}_t)} \right\rangle}{\left\langle \dfrac{1}{d_t(\mathbf{r}_t)} \right\rangle^2 \left\langle \dfrac{1}{c_t^2(\mathbf{r}_t)} \right\rangle^2} - 1, \tag{A4}$$

the variances by

$$\mathrm{Var}(\Gamma_d(\mathbf{r}_t)) = \langle \Gamma_d^2(\mathbf{r}_t) \rangle - \langle \Gamma_d(\mathbf{r}_t) \rangle^2 \tag{A5}$$

and

$$\mathrm{Var}(\Gamma_\kappa(\mathbf{r}_t)) = \langle \Gamma_\kappa^2(\mathbf{r}_t) \rangle - \langle \Gamma_\kappa(\mathbf{r}_t) \rangle^2, \tag{A6}$$

and their covariance by

Galinde *et al.*: Range-dependent waveguide reverberation model

$$\text{Cov}(\Gamma_\kappa, \Gamma_d) = \left\langle \left(1 - \frac{\bar{d}}{d_t(\mathbf{r}_t)}\right)\left(\frac{\kappa_t(\mathbf{r}_t)}{\bar{\kappa}} - 1\right)\right\rangle$$

$$= \bar{d}\left\langle \frac{1}{d_t(\mathbf{r}_t)}\right\rangle - \frac{\bar{d}}{\bar{\kappa}}\left\langle \frac{1}{d_t^2(\mathbf{r}_t)c_t^2(\mathbf{r}_t)}\right\rangle, \qquad \text{(A7)}$$

where

$$\bar{\kappa} = \left\langle \frac{1}{d_t(\mathbf{r}_t)}\right\rangle\left\langle \frac{1}{c_t^2(\mathbf{r}_t)}\right\rangle. \qquad \text{(A8)}$$

Table I provides a summary of these calculations for the New Jersey Strataform.

[1] N. C. Makris, P. Ratilal, D. Symonds, S. Jagannathan, S. Lee, and R. Nero, "Fish population and behavior revealed by instantaneous continental-shelf-scale imaging," Science **311**, 660–663 (2006).

[2] P. Ratilal, Y. Lai, D. T. Symonds, L. A. Ruhlmann, J. Goff, C. W. Holland, J. R. Preston, E. K. Scheer, M. T. Garr, and N. C. Makris, "Long range acoustic imaging of the Continental Shelf Environment: The Acoustic Clutter Reconnaisance Experiment 2001," J. Acoust. Soc. Am. **117**, 1977–1998 (2005).

[3] J. A. Goff, D. J. P. Swift, C. S. Duncan, L. A. Mayer, and J. Hughes-Clark, "High resolution swath sonar investigation of sand ridge, dune and ribbon morphology in the offshore environment of the New Jersey margin," Mar. Geol. **161**, 307–337 (1999).

[4] M. D. Collins, "A split-step Pad solution for the parabolic equation method," J. Acoust. Soc. Am. **93**, 1736–1742 (1993).

[5] P. D. Mourad and D. R. Jackson, "A model/data comparison for low-frequency bottom backscatter," J. Acoust. Soc. Am. **94**, 344–358 (1993).

[6] P. C. Hines, "Theoretical model of in-plane scatter from a smooth sediment seabed," J. Acoust. Soc. Am. **99**, 836–844 (1996).

[7] T. Yamamoto, "Acoustic scattering in the ocean from velocity and density fluctuations in the sediments," J. Acoust. Soc. Am. **99**, 866–879 (1996).

[8] B. H. Tracey and H. Schmidt, "A self-consistent theory for seabed volume scattering," J. Acoust. Soc. Am. **106**, 2524–2534 (1999).

[9] A. Ivakin, "A unified approach to volume and roughness scattering," J. Acoust. Soc. Am. **103**, 827–837 (1998).

[10] D. Li, G. V. Frisk, and D. Tang, "Modeling of bottom backscattering from three-dimensional volume inhomogeneities and comparisons with experimental data," J. Acoust. Soc. Am. **109**, 1384–1397 (2001).

[11] K. D. LePage, "Spectral integral representations of volume scattering in sediments in layered waveguides," J. Acoust. Soc. Am. **108**, 1557–1567 (2000).

[12] N. C. Makris, L. Z. Avelino, and R. Menis, "Deterministic reverberation from ocean ridges," J. Acoust. Soc. Am. **97**, 3547–3574 (1995).

[13] N. C. Makris, C. S. Chia, and L. T. Fialkowski, "The bi-azimuthal scattering distribution of an abyssal hill," J. Acoust. Soc. Am. **106**, 2491–2512 (1999).

[14] C. S. Chia, N. C. Makris, and L. T. Fialkowski, "A comparison of bistatic scattering from two geologically distinct abyssal hills," J. Acoust. Soc. Am. **108**, 2053–2070 (2000).

[15] P. M. Morse and K. U. Ingard, *Theoretical Acoustics* (Princeton University Press, Princeton, NJ, 1986), Chap. 8.

[16] P. Ratilal and N. C. Makris, "Mean and covariance of the forward field propagated through a stratified ocean waveguide with three-dimensional random inhomogeneities," J. Acoust. Soc. Am. **118**, 3532–3559 (2005).

[17] J. A. Ogilvy, *Theory of Wave Scattering from Random Rough Surfaces* (IOP, Bristol, 1991), Chap. 2.

[18] *Laser Beam Propagation in the Atmosphere*, edited by J. A. Ogilvy (Springer, Berlin, 1978), p. 60.

[19] P. M. Shearer, *Introduction to Seismology* (Cambridge University Press, New York, 1999), Chap. 1.

[20] T. Chen, P. Ratilal, and N. C. Makris, "Mean and variance of the forward field propagated through three-dimensional random internal waves in a continental-shelf waveguide," J. Acoust. Soc. Am. **118**, 3560–3574 (2005).

[21] N. C. Makris and P. Ratilal, "A unified model for reverberation and submerged object scattering in a stratified ocean waveguide," J. Acoust. Soc. Am. **109**, 909–941 (2001).

[22] M. Andrews, T. Chen, S. Lee, N. C. Makris, and P. Ratilal, "Statistics of the Parseval sum, matched filter, and instantaneous single-frequency transmissions in an ocean waveguide," J. Acoust. Soc. Am. **120**, 3220 (2006).

[23] A. K. Rogers, T. Yamamoto, and W. Carey, "Experimental investigation of sediment effect on acoustic wave propagation in the shallow ocean," J. Acoust. Soc. Am. **93**, 1747–1761 (1993).

[24] J. R. Preston and D. A. Abraham, "Non-Rayleigh reverberation characteristics near 400 Hz observed on the New Jersey Shelf," IEEE J. Ocean. Eng. **29**, 215–235 (2004).

[25] N. Donabed, "Development of a calibrated bistatic Rayleigh-Born bottom reverberation model for range-dependent Continental Shelf environments," Master's of Science thesis, Northeastern University, 2006.

[26] P. Ratilal, S. Lee, Y. Lai, T. Chen, D. Symonds, N. Donabed, and N. C. Makris, "Range-dependent 3D scattering and reverberation in the shelf environment from biology, geology, and oceanography," J. Acoust. Soc. Am. **117**, 2611 (2005).

[27] P. Ratilal and N. C. Makris, "Unified model for 3-D scattering and forward propagation in a stratified ocean waveguide with random seabed inhomogeneities," J. Acoust. Soc. Am. **116**, 2527 (2004).

[28] P. Ratilal, S. Lee, and N. C. Makris, "Range-dependent reverberation modeling with the parabolic equation," J. Acoust. Soc. Am. **114**, 2302 (2003).

[29] S. Lee, P. Ratilal, and N. C. Makris, "Explaining extended linear features observed in remote sonar images of the New Jersey continental shelf break during Acoustic Clutter Experiments in 2001 and 2003," J. Acoust. Soc. Am. **115**, 2618 (2004).

[30] J. Goff, B. J. Kraft, L. A. Mayer, S. G. Schock, C. K. Sommerfield, H. C. Olson, S. P. S. Golick, and S. Nordfjord, "Seabed characterization on the New Jersey middle and outer shelf: Correlatability and spatial variability of seafloor sediment properties," Mar. Geol. **209**, 147–172 (2004).

[31] J. A. Goff, H. C. Olsen, and C. S. Duncan, "Correlation of sidescan backscatter intensity with grain-size distribution of shelf sediments, New Jersey margin," Geo-Mar. Lett. **20**, 43–49 (2000).

[32] N. C. Makris, "The effect of saturated transmission of scintillation on ocean acoustic intensity measurements," J. Acoust. Soc. Am. **100**, 769–783 (1996).

[33] J. A. Goff, J. A. Austin, S. Gulick, S. Nordfjord, B. Christensen, C. Sommerfield, H. Olson, and C. Alexander, "Recent and modern marine erosion on the New Jersey outer shelf," Mar. Geol. **216**, 275–296 (2005).

[34] G. Bar-Yehoshua, "Quantifying the effect of dispersion in continental-shelf sound propagation," Master's thesis, MIT, Cambridge, MA, 2002.

[35] P. Ratilal, Y. Lai, and N. C. Makris, "Validity of the sonar equation and Babinet's Principle for scattering in a stratified medium," J. Acoust. Soc. Am. **112**, 1797–1816 (2002).

[36] M. B. Porter and E. L. Reiss, "A numerical method for ocean acoustic normal modes," J. Acoust. Soc. Am. **76**, 244–252 (1984).